

Repaint123: Fast and High-quality One Image to 3D Generation with Progressive Controllable 2D Repainting

Junwu Zhang^{1*} Zhenyu Tang^{1*} Yatian Pang^{1,3} Xinhua Cheng¹ Peng Jin¹
 Yida Wei⁴ Munan Ning^{1,2} Li Yuan^{1,2†}
¹Peking University ²Pengcheng Laboratory ³National University of Singapore
⁴Wuhan University

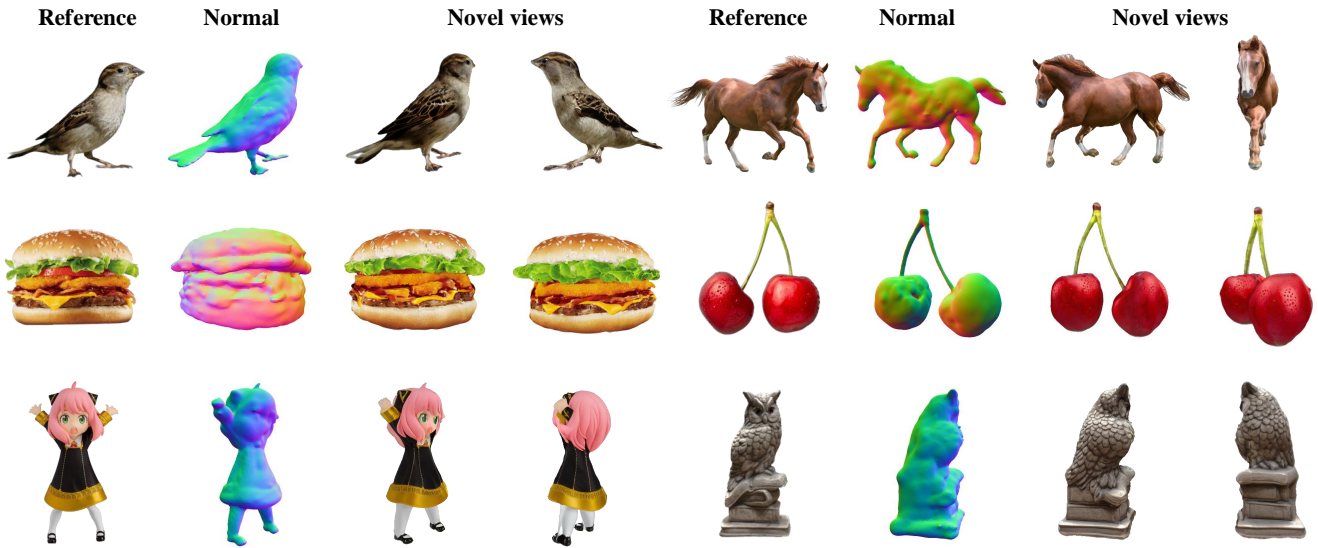


Figure 1. *Repaint123* generates high-quality 3D content with detailed texture in only **2 minutes** from a single image. *Repaint123* adopts Gaussian Splatting in the coarse stage, and then utilize a 2D controllable diffusion model with repainting strategy to generate view-consistent high-quality images. This allows for fast and high-quality refinement of the extracted mesh texture through simple MSE loss.

Abstract

Recent one image to 3D generation methods commonly adopt Score Distillation Sampling (SDS). Despite the impressive results, there are multiple deficiencies including multi-view inconsistency, over-saturated and over-smoothed textures, as well as the slow generation speed. To address these deficiencies, we present *Repaint123* to alleviate multi-view bias as well as texture degradation and speed up the generation process. The core idea is to combine the powerful image generation capability of the 2D diffusion model and the texture alignment ability of the repainting strategy for generating high-quality multi-view images with consistency. We further propose visibility-aware adaptive repainting strength for overlap regions to enhance the generated image quality in the repainting process. The gener-

ated high-quality and multi-view consistent images enable the use of simple Mean Square Error (MSE) loss for fast 3D content generation. We conduct extensive experiments and show that our method has a superior ability to generate high-quality 3D content with multi-view consistency and fine textures in **2 minutes** from scratch. Our project page is available at <https://pku-yuangroup.github.io/repaint123/>.

1. Introduction

Generating 3D content from one given reference image plays a key role at the intersection of computer vision and computer graphics [11, 17, 24, 25, 33, 35], serving as a pivotal conduit for innovative applications across fields including robotics, virtual reality, and augmented reality. Nonetheless, this task is quite challenging since it is ex-

*Equal contribution.

†Corresponding author.

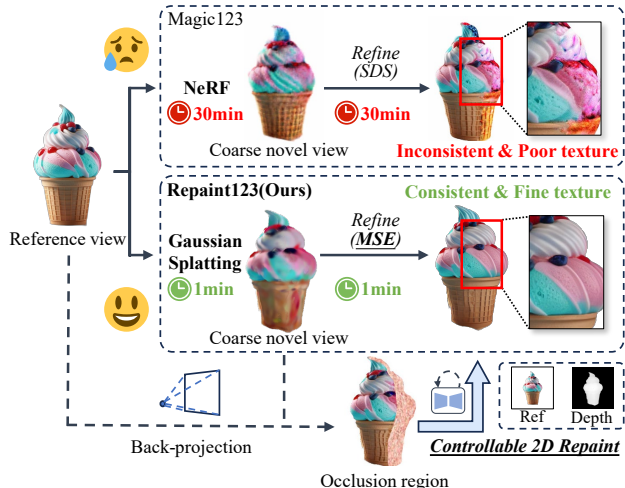


Figure 2. Motivation of our proposed pipeline. Current methods adopt SDS loss, resulting in inconsistent and poor texture. Our idea is to combine the powerful image generation capability of the controllable 2D diffusion model and the texture alignment ability of the repainting strategy for generating high-quality multi-view consistent images. The repainted images enable simple MSE loss for fast 3D content generation.

pected to generate high-quality 3D content with multi-view consistency and fine textures in a short period of time.

Recent studies [22, 24, 28, 50] utilize diffusion models [10, 39], which have notably advanced image generation techniques, to guide the 3D generation process given one reference image. Generally, the learnable 3D representation such as NeRF is rendered into multi-view images, which then are distilled by rich prior knowledge from diffusion models via Score Distillation Sampling (SDS) [34]. However, SDS may have conflicts with 3D representation optimization [16], leading to multi-view bias and texture degradation. Despite their impressive results, multiple deficiencies including multi-view inconsistency as well as over-saturated color and over-smoothed textures are widely acknowledged. Moreover, SDS is very time-consuming as a large number of optimization steps are required.

To address these deficiencies mentioned above, we propose a novel method called Repaint123 to alleviate multi-view bias as well as texture degradation and speed up the generation process. Our core idea is shown in Figure 2 refine stage. We combine the powerful image generation capability of the 2D diffusion model and the alignment ability of the repainting strategy for generating high-quality multi-view images with consistency, which enables using simple Mean Square Error (MSE) loss for fast 3D representation optimization. Specifically, our method adopts a two-stage optimization strategy. The first stage follows DreamGaussian [49] to obtain a coarse 3D model in 1 minute. In the refining stage, we first aim to generate multi-view consistent

images. For proximal multi-view consistency, we utilize the diffusion model to repaint the texture of occlusion (unobserved) regions by referencing neighboring visible textures. To mitigate accumulated view bias and ensure long-term view consistency, we adopt a mutual self-attention strategy to query correlated textures from the reference view. As for enhancing the generated image quality, we use a pre-trained 2D diffusion model with the reference image as an image prompt to perform classifier-free guidance. We further improve the generated image quality by applying adaptive repainting strengths for the overlap region, based on the visibility from previous views. As a result, with high-quality and multi-view consistent images, we can generate 3D content from these sparse views extremely fast using simple MSE loss.

We conduct extensive one image to 3D generation experiments on multiple datasets and show that our method is able to generate a high-quality 3D object with multi-view consistency and fine textures in about **2 minutes** from scratch. Compared to state-of-the-art techniques, we represent a major step towards high-quality 3D generation, significantly improving multi-view consistency, texture quality, and generation speed.

Our contributions can be summarized as follows:

- Repaint123 comprehensively considers the controllable repainting process for image-to-3d generation, preserving both the proximal view and long-term view consistency.
- We also propose to enhance the generated view quality by adopting visibility-aware adaptive repainting strengths for the overlap regions.
- Through a comprehensive series of experiments, we show that our method consistently demonstrates high-quality 3D content generation ability in **2 minutes** from scratch.

2. Related Works

2.1. Diffusion Models for 3D Generation

The recent notable achievements in 2D diffusion models [10, 39] have brought about exciting prospects for generating 3D objects. Pioneering studies [34, 52] have introduced the concept of distilling a 2D text-to-image generation model for the purpose of generating 3D shapes. Subsequent works [1, 5, 6, 9, 16, 22, 28, 35, 37, 42–44, 50, 51, 54–56, 59, 60, 63] have adopted a similar per-shape optimization approach, building upon these initial works. Nevertheless, the majority of these techniques consistently experience low efficiency and multi-face issues. In contrast to a previous study HiFi-123 [60] that employed similar inversion and attention injection techniques for image-to-3D generation, our approach differs in the selection of diffusion model and incorporation of depth prior. We utilize stable diffusion with ControlNet, introducing depth prior as an additional condition for simplicity and flexibility across

various other conditions. In comparison, HiFi-123 employs a depth-based diffusion model (stable-diffusion-2-depth) concatenating depth latent with original latent for more precise geometry control. Meanwhile, we also differ in many other aspects, like the use of repainting strategy, optimization with MSE loss, and Gaussian Splatting representation.

Recently, some works [23, 25, 26, 47] extend 2D diffusion models from single-view images to multi-view images to generate multi-view images for reconstruction, while these methods usually suffer from low-quality textures as the multi-view diffusion models are trained on limited and synthesized data.

2.2. Controllable Image Synthesis

One of the most significant challenges in the field of image generation has been controllability. Many works have been done recently to increase the controllability of generated images. ControlNet [61] and T2I-adapter [31] attempt to control the creation of images by utilizing data from different modalities. Some optimization-based methods [30, 40] learn new parameters or fine-tune the diffusion model in order to control the generation process. Other methods [3, 57] leverage the attention layer to introduce information from other images for gaining better control.

2.3. 3D Representations

Neural Radiance Fields (NeRF) [29], as a volumetric rendering method, has gained popularity for its ability to enable 3D optimization [2, 4, 7, 14, 21] under 2D supervision, while NeRF optimization can be time-consuming. Numerous efforts [32, 41] for spatial pruning have been dedicated to accelerating the training process of NeRF on the reconstruction setting. However, they fail in the generation setting of NeRF. Recently, 3D Gaussian Splatting [8, 18, 49, 58] has emerged as an alternative 3D representation to NeRF and has shown remarkable advancements in terms of both quality and speed, offering a promising avenue.

3. Preliminary

3.1. DDIM Inversion

DDIM [46] transforms random noise \mathbf{x}_T into clean data \mathbf{x}_0 over a series of time steps, by using the deterministic DDIM sampling in the reverse process, i.e., $\mathbf{x}_{t-1} = (\alpha_{t-1}/\alpha_t)(\mathbf{x}_t - \sigma_t\epsilon_\phi) + \sigma_{t-1}\epsilon_\phi$. On the contrary, DDIM inversion progressively converts clean data to a noisy state \mathbf{x}_T , i.e., $\mathbf{x}_t = (\alpha_t/\alpha_{t-1})(\mathbf{x}_{t-1} - \sigma_{t-1}\epsilon_\phi) + \sigma_t\epsilon_\phi$, here ϵ_ϕ is the predicted noise by the UNet. This method retains the quality of the data being rebuilt while greatly speeding up the process by skipping many intermediate diffusion steps.

3.2. 3D Gaussian Splatting

Gaussian Splatting [18] presents a novel method for synthesizing new views and reconstructing 3D scenes, achieving real-time speed. Unlike NeRF, Gaussian Splatting uses a set of anisotropic 3D Gaussians defined by their locations, covariances, colors, and opacities to represent the scene. To compute the color of each pixel \mathbf{p} in the image, it utilizes a typical neural point-based rendering [19, 20]. The rendering process is as follows:

$$C(\mathbf{p}) = \sum_{i \in \mathcal{N}} c_i \alpha_i \prod_{j=1}^{i-1} (1 - \alpha_j), \quad (1)$$

$$\text{where, } \alpha_i = o_i e^{-\frac{1}{2}(\mathbf{p} - \mu_i)^T \Sigma_i^{-1} (\mathbf{p} - \mu_i)},$$

where c_i , o_i , μ_i , and Σ_i represent the color, opacity, position, and covariance of the i -th Gaussian respectively, and \mathcal{N} denotes the number of the related Gaussians.

4. Method

In this section, we introduce our two-stage framework for fast and high-quality 3D generation from one image, as illustrated in Figure 4. In the coarse stage, we adopt 3D Gaussian Splatting as the representation following DreamGaussian [49] to learn a coarse geometry and texture optimized by SDS loss. In the refining stage, we convert the coarse model to mesh representation and propose a progressive, controllable repainting scheme for texture refinement. First, we obtain the view-consistency images for novel views by progressively repainting the invisible regions relative to previously optimized views with geometry control and the guidance from reference image (see Section 4.1). Then, we employ image prompts for classifier-free guidance and design an adaptive repainting strategy for further enhancing the generation quality in the overlap regions (see Section 4.2). Finally, with the generated view-consistent high-quality images, we utilize simple MSE loss for fast 3D content generation (see Section 4.3).

4.1. Multi-view Consistent Images Generation

Achieving high-quality image-to-3D generation is a challenging task because it necessitates pixel-level alignment in overlap regions while maintaining semantic-level and texture-level consistency between reference view and novel views. To achieve this, our key insight is to progressively repaint the occlusions with the reference textures. Specifically, we first delineate the overlaps and occlusions between the reference-view image and a neighboring novel-view image. Inspired by HiFi-123 [60], we invert the coarse novel-view image to deterministic intermediate noised latents by DDIM Inversion [46] and then transfer reference textures through reference attention feature injection [3]. The inversion preserves coarse 3D consistent color information

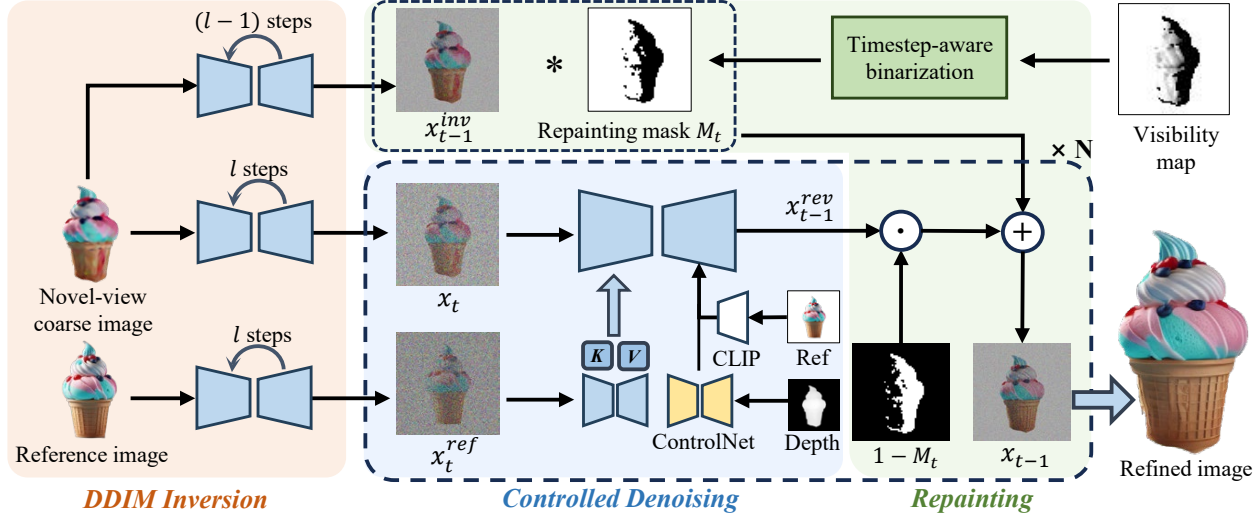


Figure 3. Controllable repainting scheme. Our scheme employs DDIM Inversion [46] to generate deterministic noisy latent from coarse images, which are then refined via a diffusion model controlled by depth-guided geometry, reference image semantics, and attention-driven reference texture. We binarize the visibility map into an overlap mask by the timestep-aware binarization operation. Overlap regions are selectively repainted during each denoising step, leading to the high-quality refined novel-view image.

in occlusions while the attention injection replenishes consistent high-frequency details. Subsequently, we iteratively denoise and blend the noised latent using inverted latents for neighbor harmony and pixel-level alignment in overlaps. Finally, we bidirectionally rotate the camera and progressively apply this repainting process from the reference view to all views. By doing this, we can seamlessly repaint occlusions with both short-term consistency (overlaps alignment and neighbor harmony) and long-term consistency (back-view consistency of semantics and textures).

Obtaining Occlusion Mask. To get the occlusion mask M_n in the novel view with the rendered image I_n and depth map D_n , given a repainted reference view with I_r and D_r , we first back-project the 2D pixels in the view V_r into 3D points P_r by scaling camera rays of V_r with depth values D_r . Then, we render a depth map D'_n from P_r and the target perspective V_n . Regions with dissimilar depth values between the two novel-view depth maps (D_n and D'_n) are occlusion regions in occlusion mask M_n .

Performing DDIM Inversion. As shown in the red part of Figure 3, to utilize the 3D-consistent coarse color and maintain the textures in overlap regions, we perform DDIM inversion on the novel-view image I to get the intermediate deterministic latents x^{inv} . With the inverted latents, we can denoise reversely to reconstruct the input image faithfully.

Repainting the Occlusions with Depth Prior. As shown in Figure 3, with the inverted latents, we can replace the overlap parts in the denoised latents during each denoising step to enforce the overlapped regions unchanged while

harmonizing the occlusion regions:

$$x_{t-1} = x_{t-1}^{inv} \odot (1 - M) + x_{t-1}^{rev} \odot M, \quad (2)$$

where $x_{t-1}^{rev} \sim \mathcal{N}(\mu_\phi(x_t, t), \Sigma_\phi(x_t, t))$ is the denoised latent of timestep t . Besides, We employ ControlNet [61] to impose additional geometric constraints from coarse depth maps to ensure the geometric consistency of images.

Injecting Reference Textures. To mitigate the cumulative texture bias at the back view, we incorporate a mutual self-attention mechanism [3] that injects reference attention features into the novel-view repainting process during each denoising step. By replacing the novel-view content features (Key features K_t and Value features V_t) with reference-view attention features (K_r and V_r), the novel-view image features can directly query the high-quality reference features by:

$$\text{Attention}(Q_t, K_r, V_r) = \text{Softmax}\left(\frac{Q_t K_r^T}{\sqrt{d}}\right) V_r, \quad (3)$$

where Q_t is the novel-view query features projected from the spatial features. This enhances texture details transfer and improves the consistency of the novel-view image.

Repainting 360° Progressively. As shown in Figure 4, we progressively sample new camera views that alternate between clockwise and counterclockwise increments. To ensure consistency in the junction of the two directions, our approach selects the nearest camera views from each of the two directions (as shown in the red cameras in Figure 4) to compute occlusion masks and repaint the texture in the novel view.

$$M = M_r \cap M_{r'}, \quad (4)$$

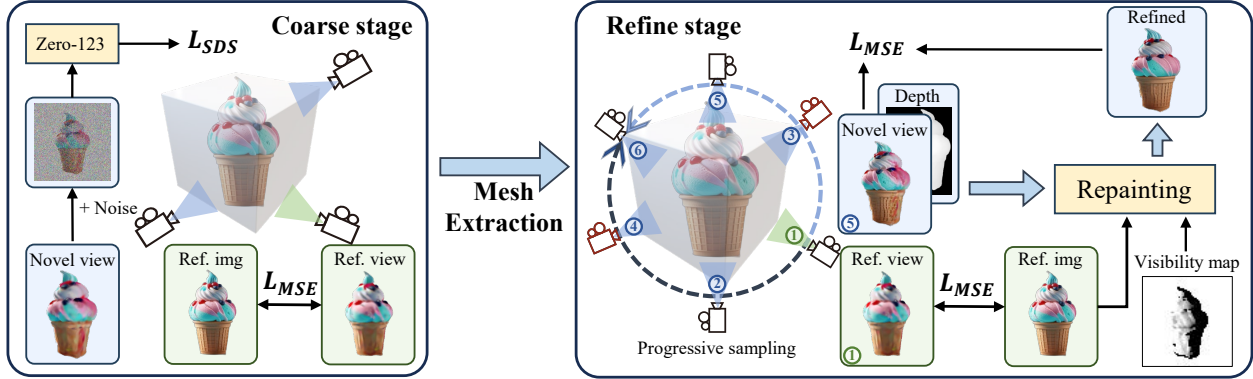


Figure 4. Image-to-3D generation pipeline. In the coarse stage, we adopt Gaussian Splatting representation optimized by SDS loss at the novel view. In the fine stage, we export Mesh representation and bidirectionally and progressively sample novel views for controllable progressive repainting. The novel-view refined images will compute MSE loss with the input novel-view image for efficient generation. Cameras in red are bidirectional neighbor cameras for obtaining the visibility map.

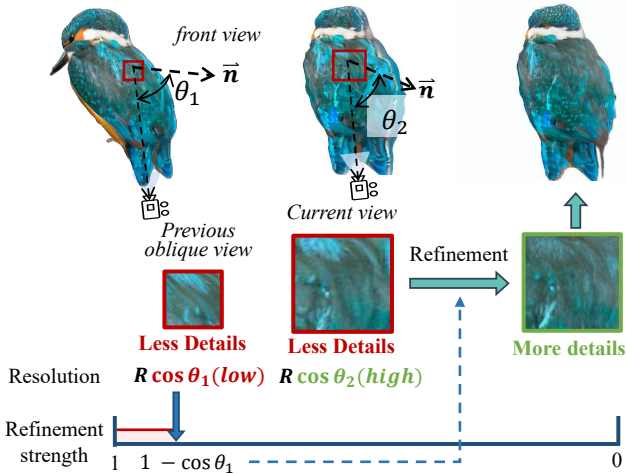


Figure 5. Relation between camera view and refinement strength. The areas in the red box are the same regions from different views.

where M_r and $M_{r'}$ are the occlusion mask obtained from two reference views, respectively and M is the final mask.

4.2. Image Quality Enhancement

Despite the progressive repainting process sustaining both short-term and long-term consistency, the accumulated texture degradation over the incremented angles can result in deteriorated multi-view image quality. We discover that the degradation is from both overlap and occlusion regions. For overlap regions, as shown in Figure 5, when the previous view is an oblique view, it leads to a low-resolution update on the texture maps, resulting in high distortion when rendering from the front view. Therefore, we propose a visibility-aware adaptive repainting process to refine the overlap regions with different strengths based on the pre-

vious best viewing angle on these regions. For occlusion regions, they achieve limited quality due to the absence of text prompts to perform classifier-free guidance [15], which is essential to diffusion models for high-quality image generation. To improve overall quality, we adopt a CLIP [36] encoder (as shown in Figure 3) to encode and project the reference image to image prompts for guidance.

Visibility-aware Adaptive Repainting. Optimal refinement strength for the overlap regions is crucial, as excessive strength produces unfaithful results while insufficient strength limits quality improvement. To select the proper refinement strength, we associate the denoising strength with the visibility map V (similar to the concept of trimap [38]). As explained in detail in Appendix 8, the visibility map is obtained based on the normal maps (i.e., the $\cos\theta$ between the normal vectors of the viewed fragments and the camera view directions) in the current view and previous views. For occlusion regions, we set the values in V to 0. For overlap regions where the current camera view provides a worse rendering angle compared to previous camera views, we set the values in V to 1, indicating these regions do not require refinement. For the remaining areas in V , we set the values to $\cos\theta^*$, which is the largest $\cos\theta$ among all previous views and indicates the best visibility during the previous optimization process. In contrast to prior approaches [38, 53] employing fixed denoising strength for all refined fragments, our work introduces a timestep-aware binarization strategy to adaptively repaint the overlap regions based on the visibility map for the faithfulness-realism trade-off. Specifically, as shown in Figure 5, we view repainting as a process similar to super-resolution that replenishes detailed information. According to the Orthographic Projection Theorem, which asserts that the projected resolution of a fragment is directly proportional to $\cos\theta$, we can assume that the repainting strength is equal to $(1 - \cos\theta^*)$.

Therefore, we can binarize the soft visibility map to the hard repainting mask based on the current timestep during each denoising step, denoted by the green box ‘‘Timestep-aware binarization’’ in Figure 3 and visualized in Figure 10:

$$M_t^{i,j} = \begin{cases} 1, & \text{if } V^{i,j} > 1 - t/T \\ 0, & \text{else,} \end{cases} \quad (5)$$

where M_t is the adaptive repainting mask, i , and j are the 2D position of the fragment in visibility map V , and T is the total number of timesteps of the diffusion model.

Projecting Reference Image to Prompts. For image conditioning, previous image-to-3D methods usually utilize textual inversion [13], which is extremely slow (several hours) for optimization and provides limited texture information due to limited number of learned tokens. Other tuning techniques, such as Dreambooth [40], require prolonged optimization and tend to overfit the reference view. Besides, vision-language ambiguity is a common issue when extracting text from the caption model. To tackle these issues, as shown in Figure 3, we adopt IP-Adapter [57] to encode and project the reference image into the image prompt of 16 tokens that are fed into an effective and lightweight cross-attention adapter in the pre-trained text-to-image diffusion models. This provides visual conditions for diffusion models to perform classifier-free guidance for enhanced quality.

4.3. Fast and High-quality 3D Generation

In the coarse stage, we adopt 3D Gaussian Splatting [18] with SDS optimization for fast generation. In the fine stage, with the controllable progressive repainting process above, we can generate view-consistent high-quality images for efficient high-quality 3D generation. The refined images are then used to directly optimize the texture through a pixel-wise MSE loss:

$$\mathcal{L}_{\text{MSE}} = \|I^{\text{fine}} - I\|_2^2, \quad (6)$$

where I^{fine} represents the refined images obtained from controllable repainting and I represent the rendered images from 3D. The MSE loss is fast to compute and deterministic to optimize, resulting in fast refinement.

5. Experiment

5.1. Implementation Details

In our experiment, we follow DreamGaussian [49] to adopt 3D Gaussian Splatting [18] representation at the coarse stage. We also explore NeRF as an alternative to Gaussian Splatting for the coarse stage, with results detailed in the Appendix. For all results of our method, we use the same hyperparameters. We progressively increment the view-points by 40 degrees, and opt to invert rendered images over 30 steps. Stable diffusion 1.5 is adopted for all experimented methods.

5.2. Baselines

We adopt RealFusion [28], Make-It-3D [50], and Zero123-XL [24], Magic123 [35] as our NeRF-based baselines and DreamGaussian [49] as our Gaussian-Splatting-based baseline. RealFusion presents a single-stage algorithm for NeRF generation leveraging an MSE loss for the reference view along with a 2D SDS loss for novel views. Make-It-3D is a two-stage approach that shares similar objectives with RealFusion but employs a point cloud representation for refinement at the second stage. Zero123 enables the synthesis of novel views conditioned on images without the need for training data, achieving remarkable quality in generating 3D content when combined with SDS. Integrating Zero123 and RealFusion, Magic123 incorporates a 2D SDS loss with Zero123 for consistent geometry and adopts DM Tet [45] representation at the second stage. DreamGaussian integrates 3D Gaussian Splatting into 3D generation and greatly improves the speed. For Zero123-XL, we adopt the implementation [48]. For other works, we use their officially released code for evaluation.

5.3. Evaluation Protocol

Datasets. Based on previous research, we utilized the RealFusion15 dataset [28] and test-alpha dataset collected by Make-It-3D [50], which comprises many common things.

Evaluation metrics. An effective 3D generation approach should closely resemble the reference view, and maintain consistency of semantics and textures with the reference when observed from new views. Therefore, to evaluate the overall quality of the generated 3D object, we choose the following metrics from two aspects: 1) PSNR and LPIPS [62], which measure pixel-level and perceptual generation quality respectively at the reference view; 2) CLIP similarity [36] and contextual distance [27], which assess the similarity of semantics and textures respectively between the novel perspective and the reference view.

5.4. Comparisons

Quantitative Comparisons. As shown in Table 1, we evaluate the quality of generated 3D objects across various methods. Our method achieves superior 3D consistency in generating 3D objects, as evidenced by best performance from CLIP-similarity and contextual distance metrics. Although our method achieves better reference-view reconstruction results than DreamGaussian, there is a gap compared with Nerf-based approaches, which we attribute to the immaturity of current Gaussian-Splatting-based methods. Compared with Nerf-based methods for the optimization time, our approach reaches a significant acceleration of over 10 times and simultaneously achieves high quality.

Qualitative Comparisons. Figure 6 displays the qualitative comparison results between our method and the baseline, while Figure 1 shows multiple novel-view images gen-

Reference	Realfusion	Make-it-3D	Zero-123-xl*	Magic123	Dreamgaussian	Ours
						
						
						
						
						
						
						
						
						
Avg. Time Reference	20min Realfusion	1h Make-it-3D	30min Zero-123-xl*	1h (+2h) Magic123	2min Dreamgaussian	2min Ours

Figure 6. Qualitative comparisons on image-to-3D generation. Zoom in for texture details.

Dataset	Metrics \ Methods	NeRF-based				Gaussian-Splatting-based	
		RealFusion	Make-it-3D	Zero-123-XL*	Magic123	DreamGaussian	Repaint123
RealFusion15	CLIP-Similarity↑	0.71	0.81	0.83	0.82	0.77	0.85
	Context-Dis↓	2.20	1.82	1.59	1.64	1.61	1.55
	PSNR↑	19.24	16.56	19.56	19.68	18.94	<u>19.00</u>
	LPIPS↓	0.194	0.177	0.108	0.107	0.111	0.101
Test-alpha	CLIP-Similarity↑	0.68	0.76	0.84	0.84	0.79	0.88
	Context-Dis↓	2.20	1.73	1.52	1.57	1.62	1.50
	PSNR↑	22.91	17.21	24.39	24.69	22.33	<u>22.38</u>
	LPIPS↓	0.105	0.237	0.050	0.046	0.057	<u>0.048</u>
	Optimization time	20min	1h	30min	1h (+2h)	2min	2 min

Table 1. We show quantitative results in terms of CLIP-Similarity↑ / Contextual-Distance↓ / PSNR↑ / LPIPS↓. The results are shown on the RealFusion15 and test-alpha datasets, while **bold** reflects the best for all methods and the **underline** represents the best for Gaussian-Splatting-based methods. * indicates that Zero123-XL adds a mesh fine-tuning stage to further improve quality. The time required by textual inversion is indicated in parentheses.

Method \ Metric	CLIP↑	Contextual↓	PSNR↑	LPIPS↓
Coarse	0.71	1.78	21.17	0.133
repaint	0.71	1.62	22.41	0.049
+mutual attention	0.78	1.56	22.42	0.048
+image prompt	0.84	1.52	22.40	0.048
+adaptive (Full)	0.88	1.50	22.38	0.048

Table 2. Quantitative ablation study on Test-alpha dataset.

erated by our methods. Repaint123 achieves the best visual results in terms of texture consistency and generation quality as opposed to other methods. From the visual comparison in Figure 6, we discover that DreamGaussian and Zero123-XL usually result in over-smooth textures, lowering the quality of the 3D object generation. Magic123 often produces inconsistent oversaturated colors in invisible areas. Realfusion and Make-It-3D fail to generate full geometry and consistent textures. This demonstrates Repaint123’s superiority over the current state of the art and its capacity to generate high-quality 3D objects in about 2 minutes.

5.5. Ablation and Analysis

In this section, we further conduct both qualitative and quantitative ablation studies (as shown in Figure 7 and Table 2) to demonstrate the effectiveness of our designs. Furthermore, we analyze the angular interval during repainting.

Effectiveness of Progressive Repainting. As shown in Figure 7, there are noticeable multi-face issues (anya) and inconsistencies in the overlap regions (ice cream). These inconsistencies are from the absence of constraints on overlap regions and can introduce conflicts and quality degradation of the final 3D generation.

Effectiveness of Mutual Attention. In Table 2, we can see that mutual attention can significantly improve the multi-view consistency and fine-grained texture consistency

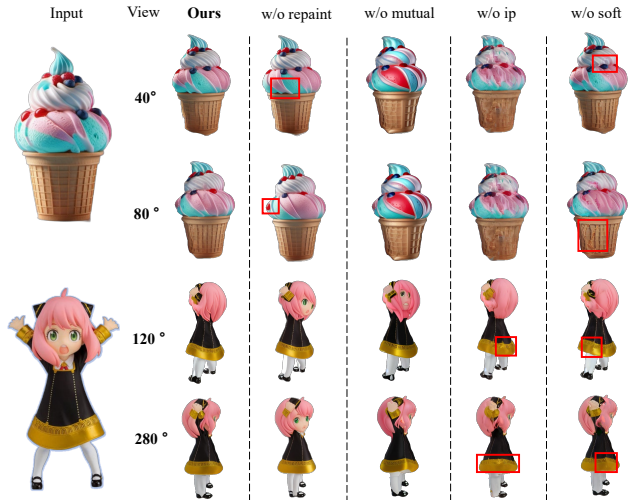


Figure 7. Qualitative ablation study. Red boxes show artifacts.

compared to vanilla repainting. As shown in Figure 7, the synthesized images without mutual attention strategy maintain the semantics but fails to transfer detailed textures from the reference image.

Effectiveness of Image Prompt. As shown in Table 2, image prompt can further improve the multi-view consistency. As shown in Figure 7 and Table 2, without an image prompt for classifier-free guidance, the multi-view images fail to generate detailed realistic and consistent textures.

Effectiveness of Adaptive Repainting. As shown in Figure 7, without the adaptive repainting mask, the oblique regions in the previous view will lead to artifacts when facing these regions due to previous low-resolution updates. Table 2 also demonstrates the effectiveness as both CLIP similarity and Contextual distance improve significantly.

Analysis of Angle Interval. We study the effect of using

Angle \ Metric	CLIP↑	Contextual↓	PSNR↑	LPIPS↓
20°	0.873	1.504	22.35	0.051
40°	0.881	1.506	22.38	0.048
60°	0.888	1.497	22.27	0.050
80°	0.885	1.487	22.26	0.051

Table 3. Effects of the chosen angle of neighboring viewpoints in Repaint123 on Test-alpha dataset.

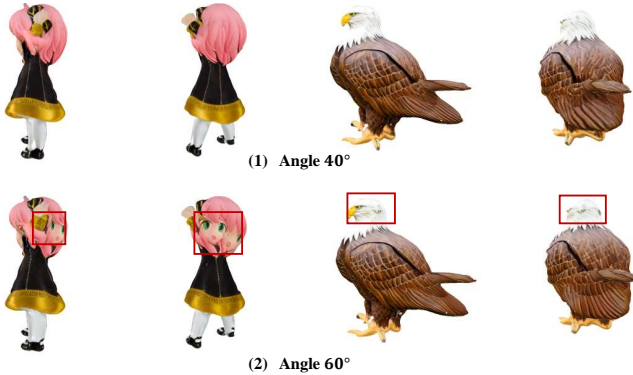


Figure 8. Visual comparison when choosing 40° and 60° as the angle interval. The red box shows the resulting multi-face issues.

different angle intervals on the performance of Repaint123 in Table 3. The table demonstrates that the metrics achieve their peak performance when the angle is set to 60 degrees. Nonetheless, Figure 8 illustrates that there is a reduced overlapping area when choosing 60 degrees as the angle interval, which consequently increases the likelihood of encountering a multi-head problem during the optimization process. Thus, we ultimately choose 40 degrees as the ideal angle interval for the optimization process.

6. Discussion

While Gaussian Splatting is fast, due to the lack of technological maturity for generation tasks and mesh extraction, it may exhibit geometry artifacts, such as holes, and achieve inferior results compared to NeRF-based methods. These issues are expected to be resolved with its development.

7. Conclusion

This work presents Repaint123 for generating high-quality 3D content from a single image in about 2 minutes. By leveraging progressive controllable repaint, our approach overcomes the limitations of existing studies and achieves state-of-the-art results in terms of both texture quality and multi-view consistency, paving the way for future progress in one image 3D content generation. Furthermore, we validate the effectiveness of our proposed method through a comprehensive set of experiments.

References

- [1] Mohammadreza Armandpour, Huangjie Zheng, Ali Sadeghian, Amir Sadeghian, and Mingyuan Zhou. Re-imagine the negative prompt algorithm: Transform 2d diffusion into 3d, alleviate janus problem and beyond. *arXiv preprint arXiv:2304.04968*, 2023. 2
- [2] Jonathan T. Barron, Ben Mildenhall, Dor Verbin, Pratul P. Srinivasan, and Peter Hedman. Mip-nerf 360: Unbounded anti-aliased neural radiance fields. *CVPR*, 2022. 3
- [3] Mingdeng Cao, Xintao Wang, Zhongang Qi, Ying Shan, Xiaohu Qie, and Yinqiang Zheng. Masactrl: Tuning-free mutual self-attention control for consistent image synthesis and editing. In *Proceedings of the IEEE/CVF International Conference on Computer Vision (ICCV)*, pages 22560–22570, 2023. 3, 4
- [4] Eric R. Chan, Connor Z. Lin, Matthew A. Chan, Koki Nagano, Boxiao Pan, Shalini De Mello, Orazio Gallo, Leonidas Guibas, Jonathan Tremblay, Sameh Khamis, Tero Karras, and Gordon Wetzstein. Efficient geometry-aware 3D generative adversarial networks. In *CVPR*, 2022. 3
- [5] Rui Chen, Yongwei Chen, Ningxin Jiao, and Kui Jia. Fantasia3d: Disentangling geometry and appearance for high-quality text-to-3d content creation. *arXiv preprint arXiv:2303.13873*, 2023. 2
- [6] Yiwen Chen, Chi Zhang, Xiaofeng Yang, Zhongang Cai, Gang Yu, Lei Yang, and Guosheng Lin. It3d: Improved text-to-3d generation with explicit view synthesis. *arXiv preprint arXiv:2308.11473*, 2023. 2
- [7] Zhiqin Chen, Thomas Funkhouser, Peter Hedman, and Andrea Tagliasacchi. Mobilenerf: Exploiting the polygon rasterization pipeline for efficient neural field rendering on mobile architectures. *arXiv preprint arXiv:2208.00277*, 2022. 3
- [8] Zilong Chen, Feng Wang, and Huaping Liu. Text-to-3d using gaussian splatting. *arXiv preprint arXiv:2309.16585*, 2023. 3
- [9] Xinhua Cheng, Tianyu Yang, Jianan Wang, Yu Li, Lei Zhang, Jian Zhang, and Li Yuan. Progressive3d: Progressively local editing for text-to-3d content creation with complex semantic prompts. *arXiv preprint arXiv:2310.11784*, 2023. 2
- [10] Prafulla Dhariwal and Alexander Nichol. Diffusion models beat gans on image synthesis. *Advances in neural information processing systems*, 34:8780–8794, 2021. 2
- [11] Zhiyang Dou, Qingxuan Wu, Cheng Lin, Zeyu Cao, Qiangqiang Wu, Weilin Wan, Taku Komura, and Wenping Wang. Tore: Token reduction for efficient human mesh recovery with transformer. In *Proceedings of the IEEE/CVF International Conference on Computer Vision*, pages 15143–15155, 2023. 1
- [12] Laura Downs, Anthony Francis, Nate Koenig, Brandon Kinman, Ryan Hickman, Krista Reymann, Thomas B McHugh, and Vincent Vanhoucke. Google scanned objects: A high-quality dataset of 3d scanned household items. In *2022 International Conference on Robotics and Automation (ICRA)*, pages 2553–2560. IEEE, 2022. 12

- [13] Rinon Gal, Yuval Alaluf, Yuval Atzmon, Or Patashnik, Amit H Bermano, Gal Chechik, and Daniel Cohen-Or. An image is worth one word: Personalizing text-to-image generation using textual inversion. *arXiv preprint arXiv:2208.01618*, 2022. 6
- [14] Peter Hedman, Pratul P. Srinivasan, Ben Mildenhall, Jonathan T. Barron, and Paul Debevec. Baking neural radiance fields for real-time view synthesis. *ICCV*, 2021. 3
- [15] Jonathan Ho and Tim Salimans. Classifier-free diffusion guidance. *arXiv preprint arXiv:2207.12598*, 2022. 5
- [16] Yukun Huang, Jianan Wang, Yukai Shi, Xianbiao Qi, Zheng-Jun Zha, and Lei Zhang. Dreamtime: An improved optimization strategy for text-to-3d content creation. *arXiv preprint arXiv:2306.12422*, 2023. 2
- [17] Heewoo Jun and Alex Nichol. Shap-e: Generating conditional 3d implicit functions. *arXiv preprint arXiv:2305.02463*, 2023. 1
- [18] Bernhard Kerbl, Georgios Kopanas, Thomas Leimkühler, and George Drettakis. 3d gaussian splatting for real-time radiance field rendering. *ACM Transactions on Graphics (TOG)*, 42(4):1–14, 2023. 3, 6
- [19] Georgios Kopanas, Julien Philip, Thomas Leimkühler, and George Drettakis. Point-based neural rendering with per-view optimization. In *Computer Graphics Forum*, pages 29–43. Wiley Online Library, 2021. 3
- [20] Georgios Kopanas, Thomas Leimkühler, Gilles Rainer, Clément Jambon, and George Drettakis. Neural point catacaustics for novel-view synthesis of reflections. *ACM Transactions on Graphics (TOG)*, 41(6):1–15, 2022. 3
- [21] Zhaoshuo Li, Thomas Müller, Alex Evans, Russell H Taylor, Mathias Unberath, Ming-Yu Liu, and Chen-Hsuan Lin. Neuralangelo: High-fidelity neural surface reconstruction. In *CVPR*, 2023. 3
- [22] Chen-Hsuan Lin, Jun Gao, Luming Tang, Towaki Takikawa, Xiaohui Zeng, Xun Huang, Karsten Kreis, Sanja Fidler, Ming-Yu Liu, and Tsung-Yi Lin. Magic3d: High-resolution text-to-3d content creation. In *CVPR*, 2023. 2
- [23] Minghua Liu, Chao Xu, Haian Jin, Linghao Chen, Zexiang Xu, Hao Su, et al. One-2-3-45: Any single image to 3d mesh in 45 seconds without per-shape optimization. *arXiv preprint arXiv:2306.16928*, 2023. 3
- [24] Ruoshi Liu, Rundi Wu, Basile Van Hoorick, Pavel Tokmakov, Sergey Zakharov, and Carl Vondrick. Zero-1-to-3: Zero-shot one image to 3d object. In *Proceedings of the IEEE/CVF International Conference on Computer Vision*, pages 9298–9309, 2023. 1, 2, 6
- [25] Yuan Liu, Cheng Lin, Zijiao Zeng, Xiaoxiao Long, Lingjie Liu, Taku Komura, and Wenping Wang. Syncdreamer: Generating multiview-consistent images from a single-view image. *arXiv preprint arXiv:2309.03453*, 2023. 1, 3
- [26] Xiaoxiao Long, Yuan-Chen Guo, Cheng Lin, Yuan Liu, Zhiyang Dou, Lingjie Liu, Yuexin Ma, Song-Hai Zhang, Marc Habermann, Christian Theobalt, et al. Wonder3d: Single image to 3d using cross-domain diffusion. *arXiv preprint arXiv:2310.15008*, 2023. 3
- [27] Roey Mechrez, Itamar Talmi, and Lihi Zelnik-Manor. The contextual loss for image transformation with non-aligned data. In *Proceedings of the European conference on computer vision (ECCV)*, pages 768–783, 2018. 6
- [28] Luke Melas-Kyriazi, Iro Laina, Christian Rupprecht, and Andrea Vedaldi. Realfusion: 360deg reconstruction of any object from a single image. In *CVPR*, 2023. 2, 6
- [29] Ben Mildenhall, Pratul P. Srinivasan, Matthew Tancik, Jonathan T. Barron, Ravi Ramamoorthi, and Ren Ng. Nerf: Representing scenes as neural radiance fields for view synthesis. In *ECCV*, 2020. 3
- [30] Ron Mokady, Amir Hertz, Kfir Aberman, Yael Pritch, and Daniel Cohen-Or. Null-text inversion for editing real images using guided diffusion models. In *Proceedings of the IEEE/CVF Conference on Computer Vision and Pattern Recognition*, pages 6038–6047, 2023. 3
- [31] Chong Mou, Xintao Wang, Liangbin Xie, Jian Zhang, Zhongqiang Qi, Ying Shan, and Xiaohu Qie. T2i-adapter: Learning adapters to dig out more controllable ability for text-to-image diffusion models. *arXiv preprint arXiv:2302.08453*, 2023. 3
- [32] Thomas Müller, Alex Evans, Christoph Schied, and Alexander Keller. Instant neural graphics primitives with a multiresolution hash encoding. *ACM TOG*, 2022. 3
- [33] Alex Nichol, Heewoo Jun, Prafulla Dhariwal, Pamela Mishkin, and Mark Chen. Point-e: A system for generating 3d point clouds from complex prompts. *arXiv preprint arXiv:2212.08751*, 2022. 1
- [34] Ben Poole, Ajay Jain, Jonathan T Barron, and Ben Mildenhall. Dreamfusion: Text-to-3d using 2d diffusion. *arXiv preprint arXiv:2209.14988*, 2022. 2
- [35] Guocheng Qian, Jinjie Mai, Abdullah Hamdi, Jian Ren, Aliaksandr Siarohin, Bing Li, Hsin-Ying Lee, Ivan Skokhodov, Peter Wonka, Sergey Tulyakov, et al. Magic123: One image to high-quality 3d object generation using both 2d and 3d diffusion priors. *arXiv preprint arXiv:2306.17843*, 2023. 1, 2, 6
- [36] Alec Radford, Jong Wook Kim, Chris Hallacy, Aditya Ramesh, Gabriel Goh, Sandhini Agarwal, Girish Sastry, Amanda Askell, Pamela Mishkin, Jack Clark, et al. Learning transferable visual models from natural language supervision. In *International conference on machine learning*, pages 8748–8763. PMLR, 2021. 5, 6
- [37] Amit Raj, Srinivas Kaza, Ben Poole, Michael Niemeyer, Nataniel Ruiz, Ben Mildenhall, Shiran Zada, Kfir Aberman, Michael Rubinstein, Jonathan Barron, et al. Dreambooth3d: Subject-driven text-to-3d generation. *arXiv preprint arXiv:2303.13508*, 2023. 2
- [38] Elad Richardson, Gal Metzger, Yuval Alaluf, Raja Giryes, and Daniel Cohen-Or. Texture: Text-guided texturing of 3d shapes. *arXiv preprint arXiv:2302.01721*, 2023. 5
- [39] Robin Rombach, Andreas Blattmann, Dominik Lorenz, Patrick Esser, and Björn Ommer. High-resolution image synthesis with latent diffusion models. In *Proceedings of the IEEE/CVF conference on computer vision and pattern recognition*, pages 10684–10695, 2022. 2
- [40] Nataniel Ruiz, Yuanzhen Li, Varun Jampani, Yael Pritch, Michael Rubinstein, and Kfir Aberman. Dreambooth: Fine tuning text-to-image diffusion models for subject-driven generation. In *Proceedings of the IEEE/CVF Conference*

- on *Computer Vision and Pattern Recognition*, pages 22500–22510, 2023. 3, 6
- [41] Sara Fridovich-Keil and Alex Yu, Matthew Tancik, Qinhong Chen, Benjamin Recht, and Angjoo Kanazawa. Plenoxels: Radiance fields without neural networks. In *CVPR*, 2022. 3
- [42] Hoigi Seo, Hayeon Kim, Gwanghyun Kim, and Se Young Chun. Ditto-nerf: Diffusion-based iterative text to omnidirectional 3d model. *arXiv preprint arXiv:2304.02827*, 2023. 2
- [43] Junyoung Seo, Wooseok Jang, Min-Seop Kwak, Jaehoon Ko, Hyeonsu Kim, Junho Kim, Jin-Hwa Kim, Jiyoung Lee, and Seungryong Kim. Let 2d diffusion model know 3d-consistency for robust text-to-3d generation. *arXiv preprint arXiv:2303.07937*, 2023.
- [44] Qihong Shen, Xingyi Yang, and Xinchao Wang. Anything-3d: Towards single-view anything reconstruction in the wild. *arXiv preprint arXiv:2304.10261*, 2023. 2
- [45] Tianchang Shen, Jun Gao, Kangxue Yin, Ming-Yu Liu, and Sanja Fidler. Deep marching tetrahedra: a hybrid representation for high-resolution 3d shape synthesis. In *Advances in Neural Information Processing Systems (NeurIPS)*, 2021. 6
- [46] Jiaming Song, Chenlin Meng, and Stefano Ermon. Denoising diffusion implicit models. *arXiv:2010.02502*, 2020. 3, 4
- [47] Stanislaw Szymanowicz, Christian Rupprecht, and Andrea Vedaldi. Viewset diffusion:(0-) image-conditioned 3d generative models from 2d data. *arXiv preprint arXiv:2306.07881*, 2023. 3
- [48] Jiayang Tang. Stable-dreamfusion: Text-to-3d with stable-diffusion, 2022. <https://github.com/ashawkey/stable-dreamfusion>. 6
- [49] Jiayang Tang, Jiawei Ren, Hang Zhou, Ziwei Liu, and Gang Zeng. Dreamgaussian: Generative gaussian splatting for efficient 3d content creation. *arXiv preprint arXiv:2309.16653*, 2023. 2, 3, 6
- [50] Junshu Tang, Tengfei Wang, Bo Zhang, Ting Zhang, Ran Yi, Lizhuang Ma, and Dong Chen. Make-it-3d: High-fidelity 3d creation from a single image with diffusion prior. In *ICCV*, 2023. 2, 6
- [51] Christina Tsalicoglou, Fabian Manhardt, Alessio Tonioni, Michael Niemeyer, and Federico Tombari. Textmesh: Generation of realistic 3d meshes from text prompts. *arXiv preprint arXiv:2304.12439*, 2023. 2
- [52] Haochen Wang, Xiaodan Du, Jiahao Li, Raymond A Yeh, and Greg Shakhnarovich. Score jacobian chaining: Lifting pretrained 2d diffusion models for 3d generation. In *Proceedings of the IEEE/CVF Conference on Computer Vision and Pattern Recognition*, pages 12619–12629, 2023. 2
- [53] Tianfu Wang, Menelaos Kanakis, Konrad Schindler, Luc Van Gool, and Anton Obukhov. Breathing new life into 3d assets with generative repainting. *arXiv preprint arXiv:2309.08523*, 2023. 5
- [54] Zhengyi Wang, Cheng Lu, Yikai Wang, Fan Bao, Chongxuan Li, Hang Su, and Jun Zhu. Prolificdreamer: High-fidelity and diverse text-to-3d generation with variational score distillation. *arXiv preprint arXiv:2305.16213*, 2023. 2
- [55] Jinbo Wu, Xiaobo Gao, Xing Liu, Zhengyang Shen, Chen Zhao, Haocheng Feng, Jingtuo Liu, and Errui Ding. Hd-fusion: Detailed text-to-3d generation leveraging multiple noise estimation. *arXiv preprint arXiv:2307.16183*, 2023.
- [56] Dejia Xu, Yifan Jiang, Peihao Wang, Zhiwen Fan, Yi Wang, and Zhangyang Wang. Neurlift-360: Lifting an in-the-wild 2d photo to a 3d object with 360 views. *arXiv e-prints*, pages arXiv–2211, 2022. 2
- [57] Hu Ye, Jun Zhang, Sibio Liu, Xiao Han, and Wei Yang. Ip-adapter: Text compatible image prompt adapter for text-to-image diffusion models. 2023. 3, 6
- [58] Taoran Yi, Jiemin Fang, Guanjun Wu, Lingxi Xie, Xiaopeng Zhang, Wenyu Liu, Qi Tian, and Xinggang Wang. Gaussian-dreamer: Fast generation from text to 3d gaussian splatting with point cloud priors. *arXiv preprint arXiv:2310.08529*, 2023. 3
- [59] Chaohui Yu, Qiang Zhou, Jingliang Li, Zhe Zhang, Zhibin Wang, and Fan Wang. Points-to-3d: Bridging the gap between sparse points and shape-controllable text-to-3d generation. *arXiv preprint arXiv:2307.13908*, 2023. 2
- [60] Wangbo Yu, Li Yuan, Yan-Pei Cao, Xiangjun Gao, Xiaoyu Li, Long Quan, Ying Shan, and Yonghong Tian. Hifi-123: Towards high-fidelity one image to 3d content generation. *arXiv preprint arXiv:2310.06744*, 2023. 2, 3
- [61] Lvmin Zhang, Anyi Rao, and Maneesh Agrawala. Adding conditional control to text-to-image diffusion models. In *Proceedings of the IEEE/CVF International Conference on Computer Vision*, pages 3836–3847, 2023. 3, 4
- [62] Richard Zhang, Phillip Isola, Alexei A Efros, Eli Shechtman, and Oliver Wang. The unreasonable effectiveness of deep features as a perceptual metric. In *CVPR*, 2018. 6
- [63] Joseph Zhu and Peiye Zhuang. Hifa: High-fidelity text-to-3d with advanced diffusion guidance. *arXiv preprint arXiv:2305.18766*, 2023. 2

Repaint123: Fast and High-quality One Image to 3D Generation with Progressive Controllable 2D Repainting

Supplementary Material

8. Visibility Map and Repainting Strength

This section delineates our proposed visibility map and its relation to the repainting strength in detail and visualization.

Obtaining Visibility Map. Figure 9 shows the process of transforming the novel-view normal map to the visibility map based on the previous neighbor-view normal map. We first conduct a back-projection of the preceding normal map into 3D points, subsequently rendering a normal map from the novel view based on these 3D points, i.e., the normal map in the projected view as shown in Figure 9. Comparing novel-view normal maps with the projected novel-view normal maps yields a high-resolution visibility map, assigning projected normal map values to areas with improved visibility in the novel view (non-white parts of visibility map in Figure 9) for further refinement and a value of 1 to other regions (white parts of visibility map in Figure 9) for preservation. The final visibility map is obtained by downsampling from 512x512 to 64x64 resolution, facilitating subsequent repainting mask generation in the latent space.

Timestep-aware Binarization. As shown in Figure 10, we visualize our proposed timestep-aware binarization process to transform the visibility map into the timestep-dependent repainting mask. Based on the proportional relation between visibility and repainting strength elucidated in Figure 3 in the main paper, the repainting region (black areas in Figure 10) can be obtained by selecting areas in the visibility map with a visibility value not exceeding $1 - t/T$, where T represents the maximum timestep during training (typically 1000), and t denotes the current repainting timestep. As illustrated in Figure 10, decreasing denoising timesteps enlarges repainting regions, indicating a progressive refinement according to prior visibility.

9. Evaluation on Multi-view Dataset

We adopt the Google Scanned Object (GSO) dataset [12] and use 10 objects for multi-view evaluation of the generated 3D objects with 3D ground truth. As shown in Table 4, the results indicate that our method is capable of generating high-quality 3D contents with multi-view consistency compared with the strong baselines.

10. Evaluation of NeRF-based Repaint123

As our repainting approach is plug-and-play for the refinement stage, we can change the representation in the coarse stage from Gaussian Splatting to NeRF. As presented in Ta-

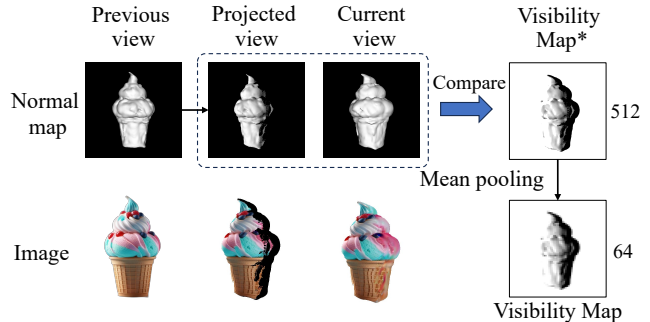


Figure 9. Visibility map creation process. The value in the normal map represents the visibility. White parts of the visibility map are less visible regions in the current view compared to the previous views, while non-white parts are more visible regions with the value of previous visibility.

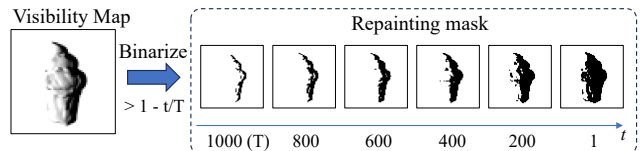


Figure 10. Timestep-aware binarization. Black areas represent repainting regions, and white areas denote preservation regions.

Method \ Metric	PSNR↑	SSIM↑	LPIPS↓	CLIP↑	Contextual↓
Syncdreamer	13.201	0.784	0.322	0.612	1.686
Magic123	14.985	0.803	0.244	0.767	1.376
Zero-123-XL	15.118	0.813	0.229	0.761	1.334
DreamGaussian	15.391	0.814	0.237	0.736	1.407
Repaint123	15.393	0.814	0.214	0.812	1.319

Table 4. Multi-view quantitative comparison with image-to-3D generation baselines on GSO dataset.

ble 5 and Figure 11, the generated 3D objects can be significantly improved by using our repainting method.

11. Ablation Study on Prompt

In this section, we conduct ablations on various prompts, including image prompt, text prompt, textual inversion, and empty prompt. As shown in Table 6, prompts significantly enhance both multi-view consistency and quality in comparison to results obtained without prompts. The efficacy stems from the classifier-free guidance. Among various prompts, image prompts demonstrate superior performance, showcasing the superior accuracy and efficiency of visual

Dataset	Metrics \ Methods	NeRF-based		Gaussian-Splatting-based	
		Magic123	Ours*	DreamGaussian	Ours
RealFusion15	CLIP-Similarity↑	0.82	0.85	0.77	0.85
	Context-Dis↓	1.64	1.57	1.61	1.55
	PSNR↑	19.68	20.27	18.94	19.00
	LPIPS↓	0.107	0.096	0.111	0.101
Test-alpha	CLIP-Similarity↑	0.84	0.88	0.79	0.88
	Context-Dis↓	1.57	1.46	1.62	1.50
	PSNR↑	24.69	24.91	22.33	22.38
	LPIPS↓	0.046	0.036	0.057	0.048

Table 5. We show quantitative results in terms of CLIP-Similarity↑ / Contextual-Distance↓ / PSNR↑ / LPIPS↓. The results are shown on the RealFusion15 and test-alpha datasets, while **bold** reflects the best for Nerf-based and Gaussian-Splatting-based methods respectively. * indicates that we adopt NeRF representation for the coarse stage.



Figure 11. Visual comparison between our NeRF-based method and Magic123.

Prompt \ Metric	PSNR↑	LPIPS↓	CLIP↑	Contextual↓
None	19.02	0.102	0.79	1.60
Text	19.00	0.102	0.83	1.58
Textual Inversion	19.01	0.101	0.84	1.57
Image	19.00	0.101	0.85	1.55

Table 6. Ablation on RealFusion15 dataset under various prompt conditions. Image prompt achieves superior performance.

prompts over text prompts, including time-consuming optimized textual prompts.

12. More Results

The videos in the supplementary material show more image-to-3D generation results of our method, demonstrat-

ing our method can produce high-quality 3D contents with consistent appearances.